

Synthesis and photoluminescence properties of $\text{Sr}_4\text{La}(\text{PO}_4)_3\text{O}:\text{RE}^{3+}$ (RE=Eu/Tb/Ce) phosphors

Ju Cheng (程菊)^{1,2}, Jia Zhang (张佳)², Hongchao Zhang (张宏超)¹, Sardar Maryam¹,
Xintian Bian (边心田)², Zhonghua Shen (沈中华)¹, Xiaowu Ni (倪晓武)¹,
and Jian Lu (陆建)^{1,*}

¹School of Science, Nanjing University of Science and Technology, Nanjing 210094, China

²School of Physics and Electronic Electrical Engineering, Huaiyin Normal University, Huai'an 223001, China

*Corresponding author: lj6805@163.com

Received August 27, 2017; accepted November 1, 2017; posted online November 27, 2017

A series of RE^{3+} (RE = Eu/Tb/Ce)-activated $\text{Sr}_4\text{La}(\text{PO}_4)_3\text{O}$ (SLPO) phosphors are synthesized with a high-temperature solid-state reaction method. The photoluminescence properties, thermal stability, morphology, and CIE values of the SLPO:Eu³⁺/Tb³⁺/Ce³⁺ phosphors are investigated. Under 394 nm excitation, the SLPO:Eu³⁺ exhibits red emission, and the SLPO:Tb³⁺ presents a green emission upon 379 nm excitation, while Ce³⁺-doped SLPO has a broad emission band ranging from 370 to 650 nm under 337 nm excitation. The investigation results indicate that the SLPO:Eu³⁺/Tb³⁺/Ce³⁺ phosphors can be effectively excited by near-ultraviolet light and may have the potential to serve as red-, green-, and blue-emitting phosphors for applications in white light-emitting diodes.

OCIS codes: 160.4760, 230.3670, 300.6170.

doi: 10.3788/COL201715.121602.

In phosphor-converted white light-emitting diodes (w-LEDs), phosphors are one of the key materials in lighting technology and have been widely investigated^[1]. The most common and simplest way to achieve white light is the combination of a blue LED chip and the yellow-emitting $\text{Y}_3\text{Al}_5\text{O}_{12}:\text{Ce}^{3+}$ (YAG:Ce) phosphor^[2]. However, this approach causes several serious problems, such as low color-rendering index (CRI, Ra ~70–80) and high correlated color temperature (CCT, ~7750 K), due to the deficiency of a red emission component^[3,4]. One solution to this problem is to make LEDs by coating a near-ultraviolet (NUV)-emitting LED with a mixture of blue-, green-, and red-emitting phosphors that could present tunable CCTs and excellent CRI values^[5]. In this case, the performance of w-LEDs strongly depends on the luminescence characters of phosphors used, so it is important to explore new phosphors with excellent luminescence properties. The apatite with the general formula $\text{M}_{10}(\text{EO}_4)_6\text{X}_2$ (M = Ca²⁺, Sr²⁺, Ba²⁺, Y³⁺, La³⁺, Gd³⁺, Mn²⁺, Na⁺, K⁺, etc.; E = P⁵⁺, Si⁴⁺, As⁵⁺, V⁵⁺, etc.; X = OH⁻, F⁻, Cl⁻, O²⁻, etc.) has been extensively studied as fluorescent lamp phosphors^[6]. $\text{Sr}_4\text{La}(\text{PO}_4)_3\text{O}$ (SLPO) is isostructural to the apatite compound. Its lattice contains different types of cationic sites, nine-fold coordinated 4f sites with C_3 point symmetry, and seven-fold coordinated 6h sites with C_s point symmetry. Sr atoms occupy both sites and La atoms are located at the 6h site^[7,8]. Both sites are suitable and can easily accommodate a great variety of rare earth (RE) ions. Compounds with apatite structure are of practical interest as efficient luminescence materials when doped with RE ions due to their high thermal stability, low sintering temperature, high chemical stability, and environmental friendliness^[9]. In

recent decades, Eu³⁺-doped apatite compounds have been used as red-emitting phosphors, such as $\text{BiCa}_4(\text{PO}_4)_3\text{O}$ ^[10] and $\text{CaLa}_4(\text{SiO}_4)_3\text{O}$ ^[11]. In addition, Tb³⁺-doped apatite compounds have also attracted great interest, such as $\text{KLaSr}_3(\text{PO}_4)_3\text{F}$ ^[12] and $\text{Ca}_2\text{Ba}_3(\text{PO}_4)_3\text{Cl}$ ^[13]. Moreover, as a lanthanide ion with the simplest electronic configuration, Ce³⁺ has a 4f¹5d⁰ ground state and a 4f⁰5d¹ excited state, and therefore shows typical 4f–5d transitions ions appearing in a large wavelength range that deeply depends on the host lattice. Apatite compounds doped with Ce³⁺ ions have also been investigated, such as $\text{Ca}_8\text{La}_2(\text{PO}_4)_6\text{O}_2$ ^[14] and $\text{Sr}_4\text{La}_2\text{Ca}_4(\text{PO}_4)_6\text{O}_2$ ^[15].

So far, the phosphate apatites have proven to be outstanding host materials for phosphors due to their good physical and chemical stability. In this work, the SLPO compound was chosen to serve as the host material in which the cation ions of Sr²⁺ and La³⁺ could provide different sites for activators of RE as well as transition metal ions. A series of SLPO:Eu³⁺/Tb³⁺/Ce³⁺ phosphors were prepared by the solid-state reaction method, and their photoluminescence (PL) properties were investigated.

Powder samples of $\text{Sr}_4\text{La}_{1-x}(\text{PO}_4)_3:x\text{Eu}^{3+}$ (SLPO: $x\text{Eu}^{3+}$, $0 \leq x \leq 0.17$), $\text{Sr}_4\text{La}_{1-x}(\text{PO}_4)_3:x\text{Tb}^{3+}$ (SLPO: $x\text{Tb}^{3+}$, $0 \leq x \leq 0.17$), and $\text{Sr}_4\text{La}_{1-x}(\text{PO}_4)_3:x\text{Ce}^{3+}$ (SLPO: $x\text{Ce}^{3+}$, $0 \leq x \leq 0.17$) were prepared by the solid-state reaction method. The starting materials included SrCO₃ (99%), (NH₄)₂HPO₄ (99%), La₂O₃ (99.99%), Eu₂O₃ (99.99%), Tb₄O₇ (99.99%), and CeO₂ (99.99%). 2wt% Li₂CO₃ (99%) was introduced as a flux. Stoichiometric amounts of the starting reagents were thoroughly mixed and ground together by an agate mortar. The mixture was first fired at 600°C for 3 h in air, reground, and calcined at 1200°C for 5 h in a reduction atmosphere

(N₂:H₂ = 95:5) for SLPO:Tb³⁺ and Ce³⁺, and in air for SLPO:Eu³⁺.

The phase purity was determined by using an ARL X'TRA powder X-ray diffractometer (XRD) with Cu K α radiation ($\lambda = 1.5406 \text{ \AA}$) operating at 40 kV and 35 mA. The PL spectra were recorded on an FS5 fluorescence spectrophotometer with a 150 W xenon lamp as the light source. The temperature-dependent measurement was carried out by an FS5 spectrofluorometer system, and the samples were mounted on a heating device whose temperature could be changed from 25°C to 200°C in 1°C increments.

Figure 1 shows the XRD patterns of the SLPO:*x*Eu³⁺/*x*Tb³⁺/*x*Ce³⁺ (*x* = 0–0.17) samples, together with the standard card data of Sr₄Bi(PO₄)₃O (JCPDS 44-0180) as a reference. Compared with the standard data, no obvious signal from impurities is observed, indicating that the as-synthesized phosphors are isostructural with Sr₄Bi(PO₄)₃O. With the increase of the doping concentration, the diffraction peaks likewise have almost no change, indicating that the doped Eu³⁺, Tb³⁺, or Ce³⁺ ions do not cause any significant changes in the crystal structure. This means that the phase formation of SLPO is not influenced by little amounts of Eu³⁺, Tb³⁺, or Ce³⁺.

In the SLPO host, there are two cationic sites, the M(I) sites are occupied by 2 Sr²⁺ cations in C₃ symmetry, while the M(II) positions with C_s symmetry could be occupied by the other 2 Sr²⁺ and La³⁺[9]. Considering the ionic radii and valence state of the cations, the Eu³⁺, Tb³⁺, or Ce³⁺ ions are expected to substitute the La³⁺ sites primarily in the SLPO lattice[6].

The PL excitation (PLE, $\lambda_{em} = 611 \text{ nm}$) and emission (PL, $\lambda_{ex} = 394 \text{ nm}$) spectra of SLPO:0.05Eu³⁺ are shown in Fig. 2. In the PLE spectrum, the broadband in the range of 240 to 320 nm is due to the charge transfer band (CTB), which is allowed by the selection rules. The sharp excitation peaks between 350 and 480 nm are attributed to the intra-4f transitions from the Eu³⁺ ground state ⁷F₀. The peaks located at 361, 382, 394, 413, and 466 nm correspond to the transitions of (⁷F₀-⁵D₄), (⁷F₀-⁵L₇), (⁷F₀-⁵L₆), (⁷F₀-⁵D₃), and (⁷F₀-⁵D₂), respectively[17,18]. The PL spectrum of SLPO:0.05Eu³⁺ under the

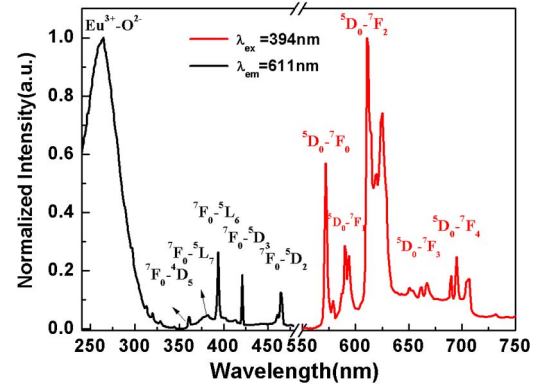


Fig. 2. (Color online) PLE ($\lambda_{em} = 611 \text{ nm}$) and emission (PL, $\lambda_{ex} = 394 \text{ nm}$) spectra of SLPO:0.05Eu³⁺ phosphor.

excitation of 394 nm has several emission peaks at 572, 594, 611, 651, and 707 nm that are assigned to the typical ⁵D₀-⁷F_{*j*} (*j* = 0–4) transitions of Eu³⁺, respectively. The most intense emission line of SLPO:0.05Eu³⁺ at 611 nm corresponds to the Eu³⁺ ⁵D₀-⁷F₂ forced electric transition, indicating the absence of inversion symmetry of the sites occupied by the Eu³⁺ ions. This agrees with the oxyapatite structure (space group, *P*₆₃/*m*), which provides low-symmetry sites for Eu³⁺ ions, i.e., the nine-coordinated 4f (C₃) site and/or seven-coordinated 6 h (Cs) site[19]. The ⁵D₀-⁷F₀ transition is a forbidden one and will be present only when Eu³⁺ occupies sites with local symmetries of C_{*n*}, C_{*nv*}, or C_{*s*}[10]. Intense emission of this ⁵D₀-⁷F₀ transition is found in the SLPO:0.05Eu³⁺ emission spectrum, which indicates that Eu³⁺ prefers to substitute La³⁺ with C_{*s*} symmetry in SLPO.

Figure 3(a) shows the emission spectra of the SLPO:*x*Eu³⁺ (*x* = 0.01, 0.05, 0.07, 0.12, and 0.17) phosphors. The shapes of the emission spectra at different Eu³⁺ ion concentrations are similar. The highest intensity of the ⁵D₀-⁷F₂ transition occurs when *x* = 0.05 in the SLPO:*x*Eu³⁺ series. To explore the concentration quenching mechanism, the critical distance (*R*_{*c*}) between the Eu³⁺ ions was calculated according to the proposed Blasse equation[20]

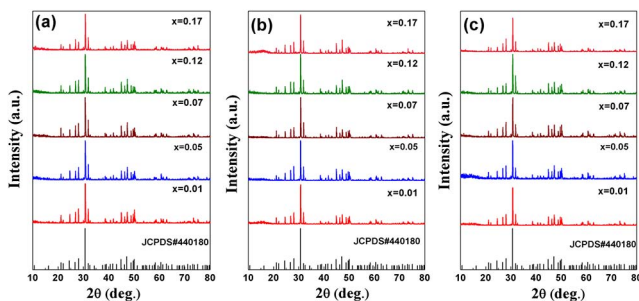


Fig. 1. XRD patterns of (a) SLPO:*x*Eu³⁺ (*x* = 0–0.17), (b) SLPO:*x*Tb³⁺ (*x* = 0–0.17), and (c) SLPO:*x*Ce³⁺ (*x* = 0–0.17).

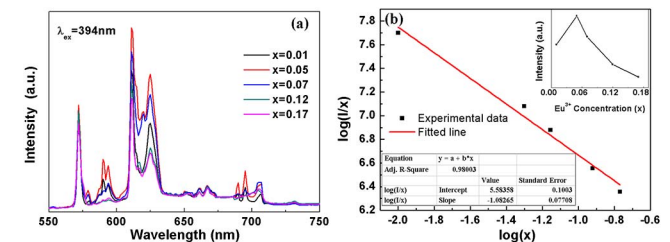


Fig. 3. (Color online) (a) Emission spectra of SLPO:*x*Eu³⁺ (*x* = 0.01, 0.05, 0.07, 0.12, and 0.17) at room temperature; (b) the relationships of $\log(x\text{Eu}^{3+})$ versus $\log(I/x\text{Eu}^{3+})$; inset: PL intensity of SLPO:*x*Eu³⁺ as a function of Eu³⁺ concentration.

$$R_c \approx 2 \left(\frac{3V}{4\pi\chi_c N} \right)^{\frac{1}{3}}, \quad (1)$$

where V is the volume of the unit cell, N is the number of cationic sites in the host lattice unit cell, and χ_c is the optimized concentration of activator ions. For the SLPO host lattice, $V = 596.05 \text{ \AA}^3$ ^[21], $N = 10$, and the optimum concentration of Eu^{3+} ions in the SLPO host lattice is $\chi_c \approx 0.05$. Therefore, the R_c value was found to be about 13.16 \AA .

According to Ref. [20], nonradiative energy transfer in the luminescence of oxidic phosphors occurs by means of electric multipolar-multipolar interaction or exchange. The interaction type between sensitizers or between sensitizer and activator can be calculated by the following equation based on Dexter theory^[22]

$$\frac{I}{x} = K[1 + \beta(x)^{\frac{\theta}{3}}]^{-1}, \quad (2)$$

where I is the luminescent intensity, x is the activator concentration, and K and β ($\beta \gg 1$) are constants for a given host crystal under the same excitation condition. The type of nonradiative energy transfer can be determined by analyzing the constant θ from the formula. If $\theta = 3$, exchange coupling is the main cause of concentration quenching. Further, $\theta = 6, 8$, and 10 are assigned to electric dipole-dipole (d-d), dipole-quadrupole (d-q), and quadrupole-quadrupole (q-q) interactions, respectively^[27].

To obtain the value of θ , the concentration dependence curve [$\log(I/x)$ versus $\log(x)$] for the luminescence intensity of $\text{SLPO}:x\text{Eu}^{3+}$ at 611 nm when excited at 394 nm is shown in Fig. 3(b). The slope of the fitted straight line ($-\theta/3$) was determined to be -1.08 with a value of R^2 (0.98003). Therefore, the value of θ can be calculated to be 3.24 , which is close to 3 . This result indicates that exchange coupling should be mainly responsible for the concentration quenching of the Eu^{3+} emission center in the $\text{SLPO}:x\text{Eu}^{3+}$ phosphor.

The PLE and PL spectra of a typical $\text{SLPO}:0.07\text{Tb}^{3+}$ sample are shown in Fig. 4. By monitoring 539 nm , the broad excitation band from 240 to 300 nm could be attributed to the $4f-5d$ transition of Tb^{3+} ^[24]. In the NUV region of 300 to 400 nm , the characteristic $4f-4f$ transitions of Tb^{3+} are observed, and the strong excitation peaks located at $302, 316, 337, 345, 357, 379$, and 484 nm are attributed to the ${}^7\text{F}_6-{}^5\text{H}_6$, ${}^7\text{F}_6-{}^5\text{D}_0$, ${}^7\text{F}_6-{}^5\text{L}_7$, ${}^7\text{F}_6-{}^5\text{L}_8$, ${}^7\text{F}_6-{}^5\text{D}_2$, ${}^7\text{F}_6-{}^5\text{D}_3$, and ${}^7\text{F}_6-{}^5\text{D}_4$ transitions, respectively^[11,23].

Upon 379 nm excitation, seven obvious emission peaks at $450, 464, 485, 539, 591, 616$, and 642 nm are ascribed to the ${}^5\text{D}_3-{}^7\text{F}_3$, ${}^5\text{D}_3-{}^7\text{F}_2$, and ${}^5\text{D}_4-{}^7\text{F}_j$ ($j = 6-2$) transitions of Tb^{3+} , respectively^[11,23]. The predominant emission is located at 539 nm ; therefore, green light is observed. To determine the optimal Tb^{3+} concentration, the emission spectra of $\text{SLPO}:x\text{Tb}^{3+}$ ($x = 0.01, 0.05, 0.07, 0.12$, and 0.17) are shown in Fig. 5(a), which indicates the

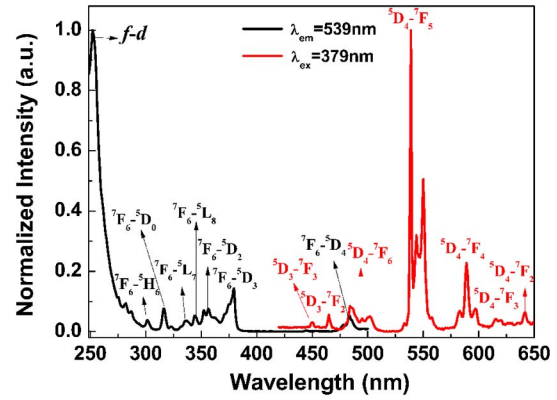


Fig. 4. (Color online) PLE ($\lambda_{\text{em}} = 539 \text{ nm}$) and emission (PL, $\lambda_{\text{ex}} = 379 \text{ nm}$) spectra of $\text{SLPO}:0.07\text{Tb}^{3+}$ phosphor.

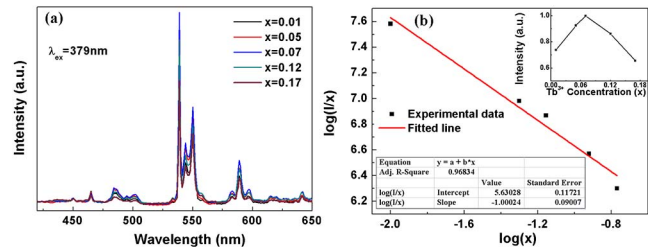


Fig. 5. (Color online) (a) Emission spectra of $\text{SLPO}:x\text{Tb}^{3+}$ ($x = 0.01, 0.05, 0.07, 0.12$, and 0.17) at room temperature; (b) the relationships of $\log(x\text{Tb}^{3+})$ versus $\log(I/x\text{Tb}^{3+})$, inset: PL intensity of $\text{SLPO}:x\text{Tb}^{3+}$ as a function of Tb^{3+} concentration.

$\text{SLPO}:0.07\text{Tb}^{3+}$ sample has the strongest emission intensity.

According to Eq. (1), the R_c value of $\text{SLPO}:x\text{Tb}^{3+}$ can be calculated to be 11.49 \AA . Figure 5(b) was proposed to determine the type of nonradiative energy transfer, from which the value of θ can be calculated to be 3.0006 . It indicates that exchange coupling should be mainly responsible for the concentration quenching of the Tb^{3+} emission center in the $\text{SLPO}:x\text{Tb}^{3+}$ phosphor.

Figure 6(a) shows the PLE and PL spectra of $\text{SLPO}:0.12\text{Ce}^{3+}$. The PLE spectrum monitored at 480 nm shows a broad absorption from 240 to 420 nm consisting of two broad bands, centered at about 290 and 340 nm , due to the $4f^7-4f^65d^1$ transition of the Ce^{3+} ions. It has a strong intensity around 330 to 350 nm , matching well with the UV-LED chips. When pumped by 337 nm , the $\text{SLPO}:0.12\text{Ce}^{3+}$ PL spectrum exhibits a broad emission band with a width of 143 nm .

Figure 6(b) shows the emission spectra of $\text{SLPO}:xCe^{3+}$ with various Ce^{3+} concentrations ($x = 0.01, 0.05, 0.07, 0.12$, and 0.17). It can be found that with the increase of Ce^{3+} content, after reaching a maximum at $x = 0.12$, the intensity declines due to the concentration quenching effect. Moreover, as the Ce^{3+} concentration increases, the emission maximum shifts to a longer wavelength. The redshift phenomenon could arise from the

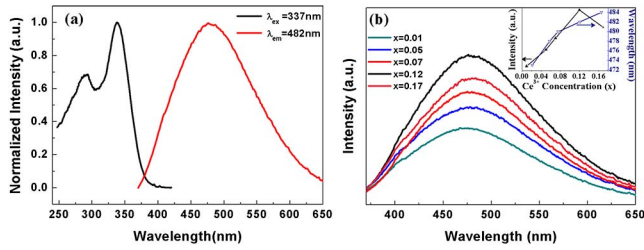


Fig. 6. (Color online) (a) PLE ($\lambda_{em} = 482$ nm) and PL ($\lambda_{ex} = 337$ nm) spectra of SLPO:0.12Ce³⁺ phosphor; (b) the PL ($\lambda_{ex} = 337$ nm) spectra of SLPO:*x*Ce³⁺ ($x = 0.01, 0.05, 0.07, 0.12, \text{ and } 0.17$) at room temperature. Inset (up left): Cell volumes of SLPO: *x*Ce³⁺ ($0.01 \leq x \leq 0.17$) as function of Ce³⁺ concentration. Inset (up right): the relationship between the emission peak with the intensity and the Ce³⁺ concentration in SLPO:*x*Ce³⁺.

following sources. First, an energy transfer from the Ce³⁺ ions at higher 5d energy levels to those at the lower energy levels, caused by the increase of Ce³⁺ concentration, will cause the energy from the 5d excited state to the 4f ground state to decrease and then the emission energy to decrease, represented by the redshift^[24]. Second, in SLPO, the dopant Ce³⁺ is expected to preferentially occupy the La³⁺ site, due to their identical valences and similar ionic radius. The up left inset of Fig. 6(b) presents the cell volumes of SLPO:*x*Ce³⁺ phosphors calculated with XRD data. It shows that when more La³⁺ ions are substituted and occupied by smaller Ce³⁺ ions, the lattice will shrink, which can lead the distances between the luminescence centers of Ce³⁺ and the ligands O²⁻ to become shorter. The relation between the crystal-field splitting D_q , and the bond length R is given as

$$D_q = \frac{Ze^2r^4}{6R^5}, \quad (3)$$

where Z is the anionic charge, e is the charge of the electron, and r is the radius of the 5d wavefunction^[25]. Thus, it can be known that the shorter Ce³⁺-O²⁻ distance R also increases the magnitude of the crystal field, so that it results in a larger split of the 5d levels, which causes the redshift of the emission wavelengths. Similar phenomenon caused by the change of crystal-field splitting in Ce³⁺-doped Sr₄La₂Ca₄(PO₄)₆O₂ and Ca₂LaZr₂Ga₃O₁₂ phosphors have been reported^[15,26].

The full width at halfmaximum (FWHM) value of about 6175 cm⁻¹ (excited at 337 nm) is relatively broad compared to the typical YAG:Ce³⁺ phosphors (~4000 cm⁻¹)^[27]. Some studies have shown that the emission spectra of the Ce³⁺-activated phosphors may be related to the site occupations of Ce³⁺ ions in the lattice^[13,14,28,29]. In order to investigate the site occupation rule of Ce³⁺ in SLPO, the emission spectra excited at different wavelengths and the excitation spectra monitored at different emission wavelengths of the sample SLPO:0.01Ce³⁺ were recorded.

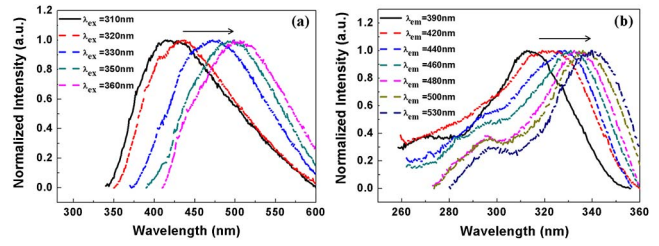


Fig. 7. (Color online) Normalized (a) PL and (b) PLE spectra of SLPO:0.01Ce³⁺ excited and monitored at different wavelengths.

Figure 7 shows the normalized PL and PLE spectra of SLPO:0.01Ce³⁺, excited and monitored at different wavelengths. It can be noted that with an increase in excitation or emission wavelength, the corresponding PL or PLE spectra show different shapes and their maximum positions gradually shift toward longer wavelengths, which indicates that Ce³⁺ is probably able to occupy more than one site in an SLPO host, even at a low concentration. When excited at 310 nm, SLPO:0.01Ce³⁺ shows a blue emission and its PL spectrum exhibits a broad band with a maximum at about 415 nm. When the excitation wavelength is 360 nm, the emission band is changed to 505 nm with a green emission. The redshift phenomenon may be due to the selective excitation of Ce³⁺ ions that occupy different sites in SLPO, and similar cases have been reported in Refs. [14,28].

The temperature dependences of luminescence for SLPO:0.05Eu³⁺, 0.07Tb³⁺, and 0.12Ce³⁺ are presented in Figs. 8(a), 8(b), and 8(c), respectively. The emission intensity decreases as the temperature increases from 25°C to 200°C.

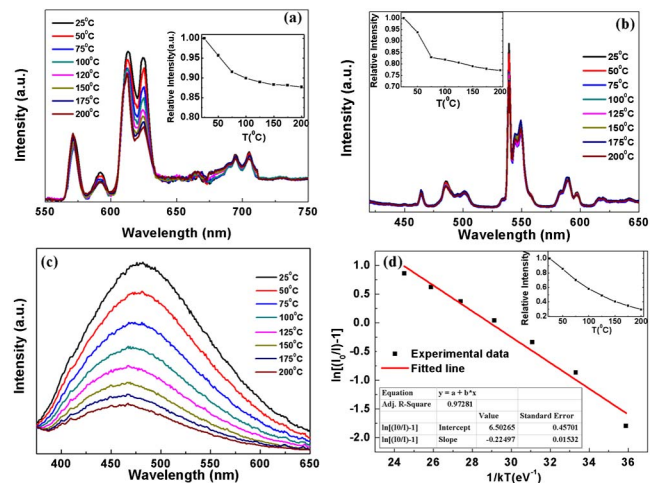


Fig. 8. (Color online) PL spectra of (a) SLPO:0.05Eu³⁺ ($\lambda_{ex} = 394$ nm) and (b) SLPO:0.07Tb³⁺ ($\lambda_{ex} = 379$ nm) at different temperatures, inset: the temperature dependence of the integrated emission intensity; (c) the PL spectra of SLPO:0.12Ce³⁺ at different temperatures ($\lambda_{ex} = 337$ nm); (d) the activation plot for thermal quenching of SLPO:0.12Ce³⁺, inset: temperature dependence of the integrated emission intensity.

With increasing measured temperature, the emission intensities of SLPO:0.05Eu³⁺ and SLPO:0.07Tb³⁺ phosphors demonstrate a gradual decrease, but the profiles of these emission spectra do not change. To observe the intensity decrease quantitatively, the corresponding temperature dependences of the Eu³⁺ and Tb³⁺ integrated emission intensities are depicted in the insets of Figs. 8(a) and 8(b), respectively. It is seen that the emission intensities of SLPO:0.05Eu³⁺ and SLPO:0.07Tb³⁺ exhibit a relatively fast decrease within the measured temperature of 100°C, but beyond this temperature the intensities change little. Compared with SLPO:0.07Tb³⁺ and SLPO:0.12Ce³⁺, the SLPO:0.05Eu³⁺ phosphor shows a more excellent thermal stability in which the relative intensity at 2000°C retains as much as 88% compared to that at 250°C.

From Figs. 8(c) and 8(d), it can be seen that the emission intensity of SLPO:0.12Ce³⁺ drops rapidly with an increase in temperature increase, and only about 41% emission intensity remains when the temperature is raised up to 150°C. This is not a very good value compared with the commercial YAG:Ce³⁺ phosphor, which is known to be a stable phosphor with a high thermal stability. Further studies will be necessary to prevent thermal quenching. The large thermal quenching behavior of Ce³⁺ in SLPO may be due to the fact that with the increase of temperature, the population of higher vibration levels and the density of phonons will increase so that nonradiative energy transfer will be more likely to occur, which can cause decreased 5d-4f transition intensity. In addition, a slight blueshift of the emission band is observed as the temperature increases. This should be ascribed to thermally active phonon-assisted tunneling from the excited states, from a lower energy in the emission band to the excited states with the higher energy emission band of Ce³⁺ in which the configuration coordinate diagram occurs^[30].

To investigate temperature quenching characteristics further, the activation energy (ΔE) was calculated using the Arrhenius equation^[31]

$$I(T) = \frac{I_0}{1 + A \exp\left(-\frac{\Delta E}{kT}\right)}, \quad (4)$$

where I_0 is the initial emission intensity, $I(T)$ is the intensity at different temperatures, ΔE is the activation energy of thermal quenching, A is a constant for a certain host, and k is the Boltzmann constant (8.629×10^{-5} eV). According to the equation, the activation energy ΔE can be obtained from the slope of the plot of $\ln [(I_0/I) - 1]$ versus $1/(kT)$. As shown in Fig. 8(d), by linear fitting, the ΔE value of Ce³⁺-doped SLPO was obtained to be 0.224 eV.

Figures 9(a), 9(b), and 9(c) show the scanning electron microscope (SEM) images of the typical SLPO:0.05Eu³⁺, SLPO:0.07Tb³⁺, and SLPO:0.12Ce³⁺ samples. The particles exhibit a relatively dispersive morphology for the

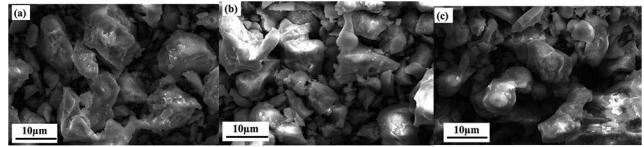


Fig. 9. SEM images of (a) SLPO:0.05Eu³⁺; (b) SLPO:0.07Tb³⁺ and (c) SLPO:0.12Ce³⁺ phosphors.

solid-state reaction preparation, but the surface of every particle is not very smooth and the particle sizes are not uniform, which is owing to the agglomeration by lots of small particles to form a big particle in the calcination process. In addition, the average particle sizes of the three phosphors were found to be around 10 µm, which can meet the requirements of w-LED phosphors.

The Commission International de l'Eclairage (CIE) chromaticity coordinates of the typical SLPO:0.05Eu³⁺, SLPO:0.07Tb³⁺, and SLPO:0.12Ce³⁺ samples were calculated from the emission spectra in the range from 550 to 750 nm, 420 to 650 nm, and 370 to 650 nm, respectively. The coordinate values and the peak emission wavelengths ($\lambda_{em-peak}$) of the three samples under different excitation wavelengths (λ_{ex}) are listed in Table 1.

The CIE coordinates of SLPO:0.05Eu³⁺ excited at 394 nm are close to the edge of the diagram shown in Fig. 10 (Point 1). Likewise, SLPO:0.07Tb³⁺ excited at 379 nm exhibits a yellowish green color, presented as Point 2. The digital photographs of the Eu³⁺- and Tb³⁺-doped SLPO samples, irradiated at 254 nm ultraviolet light, are given in the insets (a) and (b) of Fig. 10.

With the increase of the excitation wavelength, the PL spectra of SLPO:0.12Ce³⁺ also present a redshift. The CIE coordinates corresponding to SLPO:0.12Ce³⁺ excited at 312, 337, 352, 362, and 372 nm are shown in Fig. 10 (Points 3 to 7). It is apparent that from Points 3 to 7, the color turns from blue to green gradually. Inset (c) presents a digital photograph of SLPO:0.12Ce³⁺ showing green fluorescence under the ultraviolet lamp at 365 nm irradiation.

In conclusion, a series of SLPO:Eu³⁺/Tb³⁺/Ce³⁺ phosphors are synthesized with conventional solid-state

Table 1. CIE Coordinates, Peak Emission Wavelength of PL Spectra for Eu³⁺, Tb³⁺, and Ce³⁺-Doped SLPO Samples

Sample	λ_{ex}/nm	$\lambda_{em-peak}/\text{nm}$	CIE (x, y)
SLPO:0.05Eu ³⁺	394	611	(0.6405, 0.3591)
SLPO:0.07Tb ³⁺	379	539	(0.3381, 0.4445)
SLPO:0.12Ce ³⁺	312	469	(0.2316, 0.2769)
SLPO:0.12Ce ³⁺	337	482	(0.2328, 0.3014)
SLPO:0.12Ce ³⁺	352	498	(0.259, 0.3663)
SLPO:0.12Ce ³⁺	362	505	(0.2733, 0.3951)
SLPO:0.12Ce ³⁺	372	540	(0.2925, 0.4004)

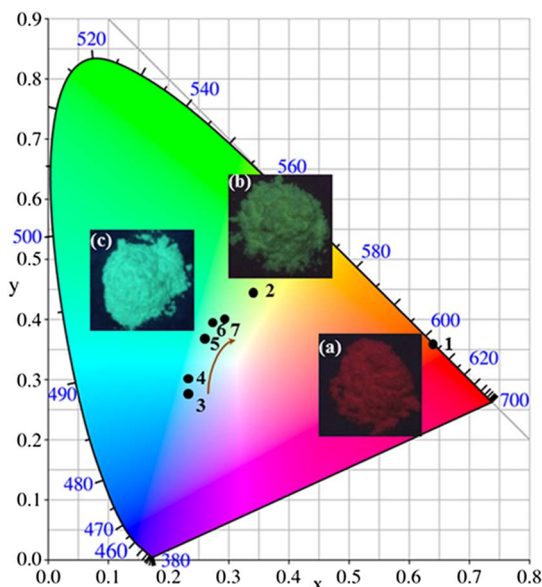


Fig. 10 CIE chromaticity diagram for SLPO:0.05Eu³⁺ (Point 1), SLPO:0.07Tb³⁺ (Point 2) and SLPO:0.12Ce³⁺ excited under different wavelengths (Points 3–7); insets: the corresponding digital photographs of (a) SLPO:0.05Eu³⁺ and (b) SLPO:0.07Tb³⁺ under 254 nm ultraviolet lamp irradiation; and (c) SLPO:0.12Ce³⁺ under 365 nm ultraviolet lamp irradiation.

reaction methods. Their luminescence properties under NUV light are investigated. The SLPO:0.05Eu³⁺ phosphor shows a red emission peak at 611 nm under an excitation of 394 nm, while SLPO:0.07Tb³⁺ displays a green emission peak at 539 nm with an excitation of 379 nm. The Ce³⁺ ions in SLPO exhibit a broad emission band from the blue to yellow region. When excited at different wavelengths, the SLPO:0.12Ce³⁺ presents various colors that may be caused by the selective excitation of Ce³⁺ ions that occupy different sites in SLPO. Studies of the temperature-dependent luminescence properties indicate that Eu³⁺- and Tb³⁺- activated SLPO phosphors have good thermal stability, while that of SLPO:0.12Ce³⁺ is relatively poor. The morphology and CIE values of the obtained phosphors are also investigated. These results indicate that the SLPO:Eu³⁺/Tb³⁺/Ce³⁺ phosphors can be promising candidates for LED applications.

This work was supported by the National Natural Science Foundation of China (NSFC) (No. 11604115) and the Educational Commission of Jiangsu Province of China (NO. 17KJA460004).

References

1. R. Li, X. Xu, L. Su, Q. Sai, C. Xia, Q. Yang, J. Xu, A. Strzep, and A. Pókoszek, *Chin. Opt. Lett.* **14**, 021602 (2016).
2. S. Ouyang, W. Zhang, Z. Zhang, Y. Zhang, and H. Xia, *Chin. Opt. Lett.* **13**, 091601 (2015).
3. Y. Shi, Y. Wang, Y. Wen, Z. Y. Zhao, B. T. Liu, and Z. G. Yang, *Opt. Express* **20**, 21656 (2012).
4. Y. Qi, L. Zhao, W. Bian, X. Yu, X. Xu, and J. Qiu, *Chin. Opt. Lett.* **15**, 081601 (2017).
5. K. Y. Jung, H. W. Lee, and H. K. Jung, *Chem. Mater.* **18**, 2249 (2006).
6. Q. Wang, Z. Ci, Y. Wang, G. Zhu, Y. Wen, and Y. R. Shi, *Mater. Res. Bull.* **48**, 1065 (2013).
7. C. Li, J. Dai, D. Deng, and S. Xu, *Optik* **127**, 2715 (2016).
8. K. B. Steinbruegge and G. D. Baldwin, *Appl. Phys. Lett.* **25**, 220 (1974).
9. G. Li, D. Geng, M. Shang, C. Peng, Z. Cheng, and J. Lin, *J. Mater. Chem.* **21**, 13334 (2011).
10. N. Lakshminarasimhan and U. V. Varadaraju, *J. Solid State Chem.* **177**, 3536 (2004).
11. J. Zhang, G. Chen, and Z. Zhai, *J. Alloys Compd.* **682**, 618 (2016).
12. Q. Guo, C. Zhao, L. Liao, H. Liu, and L. Mei, *Chemistry Select* **1**, 2883 (2016).
13. M. Shang, D. Geng, D. Yang, X. Kang, Y. Zhang, and J. Lin, *Inorg. Chem.* **52**, 3102 (2013).
14. G. Zhu, Y. Shi, M. Mikami, Y. Shimomura, and Y. Wang, *Mater. Res. Soc. Symp. Proc.* **1592**, 1 (2014).
15. G. Zhu, Y. Shi, M. Mikami, Y. Shimomura, and Y. Wang, *Opt. Mater. Express* **3**, 229 (2013).
16. R. D. Shannon, *Acta Crystallogr. A* **32**, 751 (1976).
17. Z. Wang, P. Li, Z. Yang, and Q. Guo, *Mater. Lett.* **126**, 89 (2014).
18. A. Dobrowolska, E. C. Karsu, A. J. J. Bos, and P. Dorenbos, *J. Lumin.* **160**, 321 (2015).
19. M. J. J. Lammers and G. Blasse, *J. Electrochem. Soc.* **134**, 2068 (1987).
20. G. Blasse, *Phys. Lett. A* **28**, 444 (1968).
21. G. Buvaneswari and U. V. Varadaraju, *J. Solid State Chem.* **149**, 133 (2000).
22. D. L. Dexter, *J. Chem. Phys.* **21**, 836 (1953).
23. Y. Jiang, H. Xia, S. Yang, J. Zhang, D. Jiang, C. Wang, Z. Feng, J. Zhang, X. Gu, J. Zhang, H. Jiang, and B. Chen, *Chin. Opt. Lett.* **13**, 071601 (2015).
24. J. Zhong, W. Zhuang, X. Xing, R. Liu, Y. Li, Y. Liu, and Y. Hu, *J. Phys. Chem. C* **119**, 5562 (2015).
25. P. D. Rack and P. H. Holloway, *Mater. Sci. Eng. R* **21**, 171 (1998).
26. J. Y. Zhong, W. D. Zhuang, X. R. Xing, R. H. Liu, Y. F. Li, Y. H. Liu, and Y. S. Hu, *J. Phys. Chem. C* **119**, 10 (2015).
27. G. Blasse and A. Bril, *J. Chem. Phys.* **47**, 5139 (1967).
28. W. Zhou, F. Pan, L. Zhou, D. Hou, Y. Huang, Y. Tao, H. Liang, and Y. Wang, *Inorg. Chem.* **55**, 10415 (2016).
29. R. F. Zhou, L. X. Ning, W. J. Zhou, L. T. Lin, R. Shi, and H. B. Liang, *Opt. Mater.* **66**, 1 (2017).
30. J. Zhou, Z. Xia, M. Yang, and K. Shen, *J. Mater. Chem.* **22**, 21935 (2012).
31. J. Zhang, B. Zhou, and X. Wang, *Spectrochim. Acta. A*, **165**, 85 (2016).